ARMY RESEARCH LABORATORY

Adding Liquid Payloads Effects to the 6-DOF Trajectory of Spinning Projectiles

by Gene R. Cooper

ARL-TR-5118 **March 2010**

NOTICES

Disclaimers

The findings in this report are not to be construed as an official Department of the Army position unless so designated by other authorized documents.

Citation of manufacturer's or trade names does not constitute an official endorsement or approval of the use thereof.

Destroy this report when it is no longer needed. Do not return it to the originator.

Army Research Laboratory
Aberdeen Proving Ground, MD 21005-5069

ARL-TR-5118 **March 2010**

Adding Liquid Payloads Effects to the 6-DOF Trajectory of Spinning Projectiles

Gene R. Cooper
Weapons and Materials Research Directorate, ARL

REPORT DOCUMENTATION PAGE	Form Approved OMB No. 0704-0188

1. REPORT DATE *(DD-MM-YYYY)*	2. REPORT TYPE	3. DATES COVERED (From - To)
March 2010	Final	1 October 2006–30 September 2007

4. TITLE AND SUBTITLE
Adding Liquid Payloads Effects to the 6-DOF Trajectory of Spinning Projectiles

5a. CONTRACT NUMBER

5b. GRANT NUMBER

5c. PROGRAM ELEMENT NUMBER

6. AUTHOR(S)
Gene R. Cooper

5d. PROJECT NUMBER
AH80

5e. TASK NUMBER

5f. WORK UNIT NUMBER

7. PERFORMING ORGANIZATION NAME(S) AND ADDRESS(ES)
U.S. Army Research Laboratory
ATTN: RDRL-WML-E
Aberdeen Proving Ground, MD 21005-5069

8. PERFORMING ORGANIZATION REPORT NUMBER
ARL-TR-5118

9. SPONSORING/MONITORING AGENCY NAME(S) AND ADDRESS(ES)

10. SPONSOR/MONITOR'S ACRONYM(S)

11. SPONSOR/MONITOR'S REPORT NUMBER(S)

12. DISTRIBUTION/AVAILABILITY STATEMENT
Approved for public release; distribution is unlimited.

13. SUPPLEMENTARY NOTES

14. ABSTRACT
This report outlines a relatively straightforward technique to incorporate the effect of liquid payloads on the numerical prediction of projectile trajectories. The key to this method is the addition of liquid moments imparted onto the projectile body. The first step to include the effects of liquid payloads is to model a low-viscosity liquid while undergoing typical projectile translational and angular motions. Since most projectiles carrying liquid payloads are spin stabilized with high spin rates, the moment contribution of the liquid to the angular motion of the projectile can be found using linear theory. After developing an integrated dynamic model for a projectile with a liquid payload, example trajectory characteristics are shown that exhibit typical dynamic behavior of a projectile with a liquid payload. Results comparing solid projectiles with a similar liquid-filled projectile are presented as well as a discussion of flight stability caused by a liquid payload.

15. SUBJECT TERMS
projectile dynamics, liquid payloads, rotation liquids, projectile stability, linear and nonlinear dynamics

16. SECURITY CLASSIFICATION OF:			17. LIMITATION OF ABSTRACT	18. NUMBER OF PAGES	19a. NAME OF RESPONSIBLE PERSON
a. REPORT	b. ABSTRACT	c. THIS PAGE			Gene R. Cooper
Unclassified	Unclassified	Unclassified	UU	26	19b. TELEPHONE NUMBER (*Include area code*) 410-306-0787

Standard Form 298 (Rev. 8/98)
Prescribed by ANSI Std. Z39.18

Contents

List of Figures

1. Introduction

While the bulk of projectiles in use today behave as rigid bodies while in flight, a notable number of projectiles are purposefully designed to carry a liquid payload. For example, smoke screens delivered by artillery rounds consist of a typical spin-stabilized shell containing a canister filled with white phosphorous. White phosphorous is in a liquid state when hot. Another example is new less-than-lethal projectiles having a concentric cylindrical cavity filled with liquid that delivers this payload to a target upon impact. Finally, some projectiles are designed to be general payload delivery shells, including delivery of medical supplies such as intravenous fluid bags.

Projectiles with fluid payloads have been heavily researched over the years, mainly due to the fact that these rounds can exhibit severe flight instabilities. Characteristics of this flight instability are sharp increases in projectile aerodynamic angle of attack accompanied by large changes in spin rate.[1]

Predictions of the instability induced by a liquid payload installed in a projectile have predominantly been analyzed by linear fluid dynamic theory subjected to a linear projectile coning motion. Unfortunately, these well-developed theories do not directly mesh with standard six-degree-of-freedom (6-DOF) projectile flight dynamic models. Hence, while a good deal of information is known about the effect of liquid payloads on projectiles, this information has not made its way into 6-DOF computer tools. The purpose of this report is to bridge the gap between the body of literature on effects of liquid payloads on projectiles and 6-DOF projectile flight dynamic modeling. The report begins with a review of rigid projectile flight dynamic modeling along with a description of modeling rotating liquid in a cavity. The two models are subsequently integrated such that a projectile flight dynamic model with a liquid payload results. This flight dynamic model is exercised on an example shell. Comparisons are made between a liquid-filled projectile and a similar solid projectile highlighting predictive capability of the new model.

2. Projectile Flight Dynamics

A 6-DOF rigid projectile model is employed to predict the dynamics of a projectile in flight. These equations assume a flat Earth. The 6-DOF comprises the three translational components describing the position of the projectile's center of mass and the three Euler angles describing the orientation of the projectile with respect to the Earth. Figures 1 and 2 provide a visualization of the degrees of freedom.

[1] Karpov, B. G. *Experimental Observations of the Dynamic Behavior of Liquid-Filled Shell*; BRL-TR-1171; U.S. Army Ballistics Research Laboratory: Aberdeen Proving Ground, MD, August 1961.

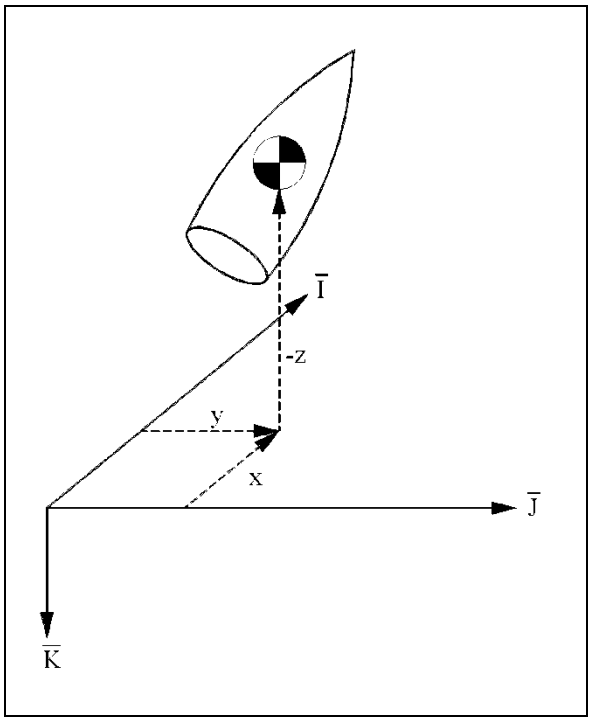

Figure 1. Projectile position coordinate definitions.

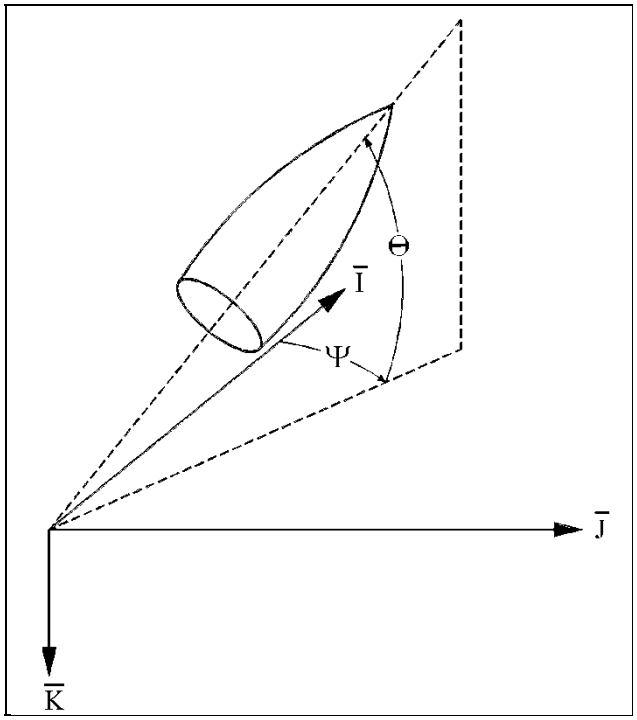

Figure 2. Projectile orientation definitions.

The equations of motion[2] for the 6-DOF model, derived in the no-roll frame, are shown in equations 1–4.

$$\begin{Bmatrix} \dot{x} \\ \dot{y} \\ \dot{z} \end{Bmatrix} = \begin{bmatrix} c_\theta c_\psi & -s_\psi & s_\theta c_\psi \\ c_\theta s_\psi & c_\psi & s_\theta s_\psi \\ -s_\theta & 0 & c_\theta \end{bmatrix} \begin{Bmatrix} \tilde{u} \\ \tilde{v} \\ \tilde{w} \end{Bmatrix}. \tag{1}$$

$$\begin{Bmatrix} \dot{\phi} \\ \dot{\theta} \\ \dot{\psi} \end{Bmatrix} = \begin{bmatrix} 1 & 0 & t_\theta \\ 0 & 1 & 0 \\ 0 & 0 & 1/c_\theta \end{bmatrix} \begin{Bmatrix} \tilde{p} \\ \tilde{q} \\ \tilde{r} \end{Bmatrix}. \tag{2}$$

$$\begin{Bmatrix} \dot{\tilde{u}} \\ \dot{\tilde{v}} \\ \dot{\tilde{w}} \end{Bmatrix} = \begin{Bmatrix} \tilde{X}/m \\ \tilde{Y}/m \\ \tilde{Z}/m \end{Bmatrix} + \begin{Bmatrix} \tilde{r}\tilde{v} - \tilde{q}\tilde{w} \\ -t_\theta \tilde{r}\tilde{w} - \tilde{r}\tilde{u} \\ \tilde{q}\tilde{u} + t_\theta \tilde{r}\tilde{v} \end{Bmatrix}. \tag{3}$$

$$\begin{Bmatrix} \dot{\tilde{p}} \\ \dot{\tilde{q}} \\ \dot{\tilde{r}} \end{Bmatrix} = [I]^{-1} \left(\begin{Bmatrix} \tilde{L} \\ \tilde{M} \\ \tilde{N} \end{Bmatrix} - \begin{bmatrix} 0 & -\tilde{r} & \tilde{q} \\ \tilde{r} & 0 & \tilde{r}t_\theta \\ -\tilde{q} & -\tilde{r}t_\theta & 0 \end{bmatrix} [I] \begin{Bmatrix} \tilde{p} \\ \tilde{q} \\ \tilde{r} \end{Bmatrix} \right). \tag{4}$$

The force acting on the projectile in equation 3 comprises the weight force (W), aerodynamic force, and liquid payload force (L). The aerodynamic force is split into a standard (A) and Magnus (M) aerodynamic force. The combination of forces is expressed in equation 5.

$$\begin{Bmatrix} \tilde{X} \\ \tilde{Y} \\ \tilde{Z} \end{Bmatrix} = \begin{Bmatrix} \tilde{X}_W \\ \tilde{Y}_W \\ \tilde{Z}_W \end{Bmatrix} + \begin{Bmatrix} \tilde{X}_A \\ \tilde{Y}_A \\ \tilde{Z}_A \end{Bmatrix} + \begin{Bmatrix} \tilde{X}_M \\ \tilde{Y}_M \\ \tilde{Z}_M \end{Bmatrix} + \begin{Bmatrix} \tilde{X}_L \\ \tilde{Y}_L \\ \tilde{Z}_L \end{Bmatrix}. \tag{5}$$

Equation 6 provides the expression for the weight force in the no-roll coordinate system.

$$\begin{Bmatrix} \tilde{X}_W \\ \tilde{Y}_W \\ \tilde{Z}_W \end{Bmatrix} = mg \begin{Bmatrix} -s_\theta \\ 0 \\ c_\theta \end{Bmatrix}. \tag{6}$$

[2]Slegers, N.; Kyle, J.; Costello, M. Nonlinear Model Predictive Control Technique for Unmanned Air Vehicles. *Journal of Guidance, Control, and Dynamics* **2006**, *29* (5), 1179–1188.

Equation 7 provides the expression for the aerodynamic force in the no-roll coordinate system. This force acts upon the projectile at the aerodynamic center of pressure.

$$\begin{Bmatrix} \tilde{X}_A \\ \tilde{Y}_A \\ \tilde{Z}_A \end{Bmatrix} = -\frac{\pi}{8}\rho {V_A}^2 D^2 \begin{Bmatrix} C_{X0} + C_{X2}\alpha^2 + C_{X2}\beta^2 \\ C_{Y0} + C_{YB1}\beta \\ C_{Z0} + C_{ZA1}\alpha \end{Bmatrix}. \tag{7}$$

Equation 8 provides the expression for the Magnus force in the no-roll coordinate system. The Magnus force acts upon the projectile at the Magnus force center of pressure.

$$\begin{Bmatrix} \tilde{X}_M \\ \tilde{Y}_M \\ \tilde{Z}_M \end{Bmatrix} = \frac{\pi}{8}\rho {V_A}^2 D^2 \begin{Bmatrix} 0 \\ \dfrac{\tilde{p}DC_{NPA}\alpha}{2V_A} \\ \dfrac{-\tilde{p}DC_{NPA}\beta}{2V_A} \end{Bmatrix}. \tag{8}$$

Equations 7 and 8 are based on Mach-number-dependent coefficients, the aerodynamic angles of attack given in equations 9 and 10, and the total aerodynamic velocity given in equation 11.

$$\tilde{\alpha} = \tan^{-1}\left(\tilde{w}_A / \tilde{u}_A\right). \tag{9}$$

$$\tilde{\beta} = \tan^{-1}\left(\tilde{v}_A / \tilde{u}_A\right). \tag{10}$$

$$V_A = \sqrt{\tilde{u}_A{}^2 + \tilde{v}_A{}^2 + \tilde{w}_A{}^2}\,. \tag{11}$$

The moment acting on the projectile in equation 4 comprises the moment due to the standard aerodynamic force (A), the moment due to the Magnus aerodynamic force (M), the unsteady aerodynamic moment (UA), and the liquid payload moment (L) as shown in equation 12.

$$\begin{Bmatrix} \tilde{L} \\ \tilde{M} \\ \tilde{N} \end{Bmatrix} = \begin{Bmatrix} \tilde{L}_A \\ \tilde{M}_A \\ \tilde{N}_A \end{Bmatrix} + \begin{Bmatrix} \tilde{L}_M \\ \tilde{M}_M \\ \tilde{N}_M \end{Bmatrix} + \begin{Bmatrix} \tilde{L}_{UA} \\ \tilde{M}_{UA} \\ \tilde{N}_{UA} \end{Bmatrix} + \begin{Bmatrix} \tilde{L}_L \\ \tilde{M}_L \\ \tilde{N}_L \end{Bmatrix}. \tag{12}$$

The moment due to the aerodynamic force is expressed in equation 13.

$$\begin{Bmatrix} \tilde{L}_A \\ \tilde{M}_A \\ \tilde{N}_A \end{Bmatrix} = \begin{bmatrix} 0 & -R_{\oplus CAZ} & R_{\oplus CAY} \\ R_{\oplus CAZ} & 0 & -R_{\oplus CAX} \\ -R_{\oplus CAY} & R_{\oplus CAX} & 0 \end{bmatrix} \begin{Bmatrix} \tilde{X}_A \\ \tilde{Y}_A \\ \tilde{Z}_A \end{Bmatrix}. \tag{13}$$

The moment due to the Magnus force is expressed in equation 14.

$$\begin{Bmatrix} \tilde{L}_M \\ \tilde{M}_M \\ \tilde{N}_M \end{Bmatrix} = \begin{bmatrix} 0 & -R_{\oplus CMZ} & R_{\oplus CMY} \\ R_{\oplus CMZ} & 0 & -R_{\oplus CMX} \\ -R_{\oplus CMY} & R_{\oplus CMX} & 0 \end{bmatrix} \begin{Bmatrix} \tilde{X}_M \\ \tilde{Y}_M \\ \tilde{Z}_M \end{Bmatrix}. \tag{14}$$

The unsteady aerodynamic moments acting on the projectile are expressed in equation 15.

$$\begin{Bmatrix} \tilde{L}_{UA} \\ \tilde{M}_{UA} \\ \tilde{N}_{UA} \end{Bmatrix} = \frac{\pi}{8} \rho {V_A}^2 D^3 \begin{Bmatrix} C_{DD} + \dfrac{\tilde{p} D C_{LP}}{2V_A} \\ \dfrac{\tilde{q} D C_{MQ}}{2V_A} \\ \dfrac{\tilde{r} D C_{NR}}{2V_A} \end{Bmatrix}. \tag{15}$$

The coefficients used in this model are projectile-specific functions of the Mach number of the projectile. For fin-stabilized projectiles, Magnus force and moment are typically ignored since their effect is rather small for slowing rolling projectiles.

The dynamic equations of motion expressed in equations 1–15 are highly nonlinear. Due to this fact, numerical integration is commonly used to obtain solutions to this initial value problem.

3. Liquid Payload Moments

Angular motion of a projectile is altered by the internal motion of the liquid payload. The liquid dynamics in this report parallel the dynamics given by Murphy[3] such that the linear projectile theory gives a second-order differential equation for $\tilde{\xi} = \tilde{\beta} + i\tilde{\alpha}$ written in terms of the lateral force and moment

[3]Murphy, C. H. *Angular Motion of a Spinning Projectile With a Viscous Liquid Payload*; ARBRL-MR-3194; U.S. Army Ballistics Research Laboratory: Aberdeen Proving Ground, MD, August 1982. (See also *Journal of Guidance, Control, and Dynamics* **1983**, *6*, 280–286.)

$$
\begin{aligned}
&\ddot{\tilde{\xi}}+\left(H-i\sigma\dot{\phi}\right)\dot{\tilde{\xi}}-\left(M+i\sigma\dot{\phi}T\right)\tilde{\xi}=0\\
&H=\frac{\pi\rho V_A D^2}{8m}\left(\tilde{p}C_{NPA}-k_y^{-2}C_{MQ}\right)\\
&M=\frac{\pi\rho V_A^2 D^3}{8Iy}C_{MA}\\
&\Sigma=\frac{\pi\rho V_A D^2}{8m}\left(\tilde{p}C_{NPA}+k_x^{-2}\tilde{p}C_{MPA}\right)\\
&\sigma=Ix/Iy.
\end{aligned}
\tag{16}
$$

Solving this last equation gives the linear sum of two complex polar arms:

$$
\tilde{\xi}=K_1\,e^{iT_1 P t}+K_2\,e^{iT_2 P t},
\tag{17}
$$

where

$\ln\left(K_j/K_{j0}\right)=\varepsilon_j T_j P t$,

$T_j=\sigma/2\left[1\pm\sqrt{1-1/S_g}\right]$,

$S_g=\sigma^2P^2/4M$ if $|H|<<1, |\Sigma|<<1$, and

$\varepsilon_j=-\dfrac{T_jH-\sigma\Sigma}{\left(2T_j-\sigma\right)T_jP}$.

Consider a projectile containing a liquid-filled cavity subjected to the angular motion of a free-flight projectile. This angular motion generates inertial waves in the contained liquid, which, in turn, impacts the projectile angular motion since liquid moments are now acting on the projectile. The assumption is made that liquid moments are small enough so the linear theory assumptions used to obtain equation 16 are not violated.

X,Y,Z and $X,\tilde{Y},\tilde{Z}$ are respectively body and nonrolling coordinate systems, where the x-axis is the projectile's symmetry axis. The earth-fixed axes X_E,Y_E,Z_E has X_E initially along the velocity vector and $\tilde{Z},Z_E$ are initially downward.

Moments due to the liquid payload are assumed to be caused by the coning motions; the linear response of these moments is modeled as[3,4]

$$
\tilde{M}_L+i\,\tilde{N}_L=m_L\,a^2\,P^2\left[T_1\,C_{LM_1}\,K_1\,e^{i\phi_1}+T_2\,C_{LM_2}\,K_2\,e^{i\phi_2}\right].
\tag{18}
$$

[4]Cooper, G. R. *Moment Exerted on Coning Projectile by a Spinning Liquid in a Cylindrical Cavity Containing a Porous Medium*; ARBRL-MR-3677; U.S. Army Ballistics Research Laboratory: Aberdeen Proving Ground, MD, June 1988.

C_{LM_j} will depend on time, T_j, ε_j, the shape of the cavity, Reynolds number, and the direction of spin. Note that the factor(s) T_j are introduced because the liquid moments will vanish when $T_j = 0$. Furthermore, C_{LM_j} causes rotations in the plane of $\exp(i\phi_j)$ as well as rotations out of the plane, so the following definition is introduced:

$$C_{LM_j} = C_{LSM_j} + i\,C_{LIM_j}, \tag{19}$$

where C_{LSM_j} and C_{LIM_j} are real and represent the liquid side moment and the liquid in-plane moment coefficients, respectively.[3]

Combining the payload moment of equation 19 with the aerodynamic force and moment produces a slightly more complicated differential equation[3] for $\tilde{\xi}$. The projectile angular motion continues to be an epicycle of equation 16, which causes the frequency and damping to take the forms

$$\begin{aligned}
T_j &= T_{0j} + T_{2j}\,C^2_{LSM_j} \\
T_{0j} &= \sigma/2\left[f_j - (-1)^j\sqrt{f_j^2 - 1/S_g}\right] \\
T_{2j} &= \frac{\left((f_j - 1)\sigma C_{Lsm}\,T_{0j}\right)^2}{C^2_{LIM_j}\left(2T_{0j} - \sigma\right)^2\left(2T_{0j} - f_j\sigma\right)} \\
f_j &= 1 + \left(m_L a^2/I_x\right)C_{LIM_j} \\
\varepsilon_j &= \varepsilon_{aj} + C_{LSM_j}\left(m_L\,a^2/I_x\right)\left(2T_j/\sigma - 1\right)^{-1}.
\end{aligned} \tag{20}$$

The last equation shows that C_{LSM_j} has the same effect on damping angular motion as does the aerodynamic damping moment. Since the coefficient C_{LSM_j} is usually positive for the fast mode, this means that $C_{LSM_j} > 0$ and will hence undamp the motion. Similarly, negative C_{LSM_j} will undamp the slow mode.

In addition to the two transverse liquid moments (which Murphy[5] has shown), the axial liquid moment $\tilde{L}$ takes the form

$$\begin{aligned}
\tilde{L} &= m_L\,a^2\,\dot{\phi}^2\,T_j\,K_j^2\,C_{LRM_j} \\
C_{LRM_j} &= -C_{LSM_j} + \frac{T\varepsilon_j}{2}\left[1 - \frac{4c^2}{3a^2}\right],
\end{aligned} \tag{21}$$

[5]Murphy, C. H. *Liquid Payload Roll Moment Induced by a Spinning and Coning Projectile*; ARLBR-TR-02521; U.S. Army Ballistics Research Laboratory: Aberdeen Proving Ground, MD, September 1983.

thus the roll moment is obtained directly from the liquid side moment calculation.

When analyzing the impact of inertial waves, it is convenient to consider only that part of the moment exerted by the liquid due to only one of the two projectile coning frequencies T_j. For steady-state linear motion, this part will be the total liquid moment, but for unsteady or nonlinear liquid motion, this part will be an average contribution of the actual liquid moment. Thus, the total liquid moment will be the sum of two averaged liquid moments.

4. Liquid Motion Model

The linear liquid analysis used for this study is identical to the analysis given by Murphy[3] and thus only a cursory review is presented here. Consider a projectile with a cylindrical payload cavity with radius, a, and height $2c$. The cylinder's axis is collinear with the projectile axis with its center located at the projectile's center of mass. Linear theory is used to predict the liquid moment caused by coning motion, which has the form

$$\tilde{\xi} = K_j e^{i\phi_j} = \hat{K} e^{s\phi} \quad (j = 1, 2), \tag{22}$$

where

$\tilde{\xi} = K_j e^{i\phi_j} = \hat{K} e^{s\phi}$,

$s = (\varepsilon_j + i) T_j$,

$\phi = \dot{\phi} t$, and

$\hat{K} = K_{j0} e^{i\phi_{j0}} \quad (j = 1, 2)$.

The liquid motion is approximated quasi-statically as the sum of two steady-state projectile coning motions. The liquid velocity components and liquid pressure have the same dependency on time and θ as the velocity components of points on the coning projectile.[3] Thus, four small dimensionless functions, v, w, u, p of r and x, are introduced:

$$\begin{aligned}
V_r &= R\left(v e^{jst - i\theta}\right)\left(a\dot{\phi}\right) \\
V_\theta &= \left[R\left(w e^{jst - i\theta}\right) + r\dot{\phi}\right]\left(a\dot{\phi}\right) \\
V_x &= R\left(u e^{jst - i\theta}\right)\left(a\dot{\phi}\right) \\
\hat{P} &= \left[R\left(p e^{jst - i\theta}\right) + \dot{\phi}^2 r^2/2\right]\left(\rho_L a^2 \dot{\phi}^2\right),
\end{aligned} \tag{23}$$

for the liquid cylindrical velocity components V_r, V_θ, V_x, and pressure $\hat{P}$. These are placed in the linearized Navier-Stokes equations and the continuity equation to yield

$$
\begin{aligned}
(s-i)v - 2w + a\frac{\partial p}{\partial r} &= Re^{-1}\left[\Delta_\theta^2 v - \frac{a^2 v}{r^2} + \frac{2a^2 i w}{r^2}\right] \\
(s-i)w + 2v - \frac{i a p}{r} &= Re^{-1}\left[\Delta_\theta^2 w - \frac{a^2 w}{r^2} - \frac{2a^2 i v}{r^2}\right] \\
(s-i)u + a\frac{\partial p}{\partial x} &= Re^{-1}\Delta_\theta^2 u \\
\frac{\partial r v}{\partial r} - i w + r\frac{\partial u}{\partial x} &= 0 \quad ,
\end{aligned}
\tag{24}
$$

where

$$\Delta_\theta^2 = a^2\left[\frac{\partial^2}{\partial r^2} + \frac{\partial}{r\,\partial r} + \frac{\partial^2}{\partial x^2} - \frac{1}{r^2}\right].$$

These equations are solved by assuming the liquid has low viscosity so viscous effects can be ignored except for high-gradient boundary layers near the cylinder walls. This means the inverse Reynolds number is taken to be very small, $Re^{-1} << 1$, so inertial wave solutions are modeled as the sum of inviscid, $Re^{-1} = 0$, contributions plus viscous boundary layer contributions of order $1/\sqrt{Re}$.

$$
\begin{aligned}
v &= v_I + v_v \\
w &= w_I + w_v \\
u &= u_I + u_v \\
p &= p_I + p_v \, .
\end{aligned}
\tag{25}
$$

Order of magnitude arguments applied to equation 25 when substituted in equation 24 show the boundary layer solutions near $r = a$ have the following form:

$$
\begin{aligned}
w_v &= \left[(1+is)x/a\,\hat{K} - w_I\right]e^{(r/a-1)/\delta_a} \\
u_v &= \left[(i-s)\hat{K} + u_I\right]e^{(r/a-1)/\delta_a} \\
p_v &= \frac{2}{a}\int w_v \, dr \\
v_I - a\,\delta a\frac{\partial v_I}{\partial r} &= (i-s)\frac{x}{a} \ , \ \text{at } r = a \ .
\end{aligned}
\tag{26}
$$

Near the end walls one will find

$$
\begin{aligned}
w_v + i\,u_v &= -\left(w_I + i\,u_I\right) e^{\alpha(1\mp x/c)} \\
w_v - i\,u_v &= \left[w_I - i\,u_I \mp 2\left(i+s\right)\frac{c}{a}\hat{K} \right] e^{\beta(1\mp x/c)} \\
p_v &= 0 \\
u_I \mp \delta_c\, c\frac{\partial u_I}{\partial x} &= -i\left(1+is\right)\frac{r}{a}\hat{K} \text{ at } x = \pm c \quad .
\end{aligned}
\tag{27}
$$

Note that $\left[w_v, u_v, p_v\right] \to 0$ exponentially with distance from the container walls; the details regarding these solutions are explained in an appendix in Murphy.[3]

5. Liquid Moments

The major components of the liquid moment are due to the pressure on the walls of the container, and the viscous shear produces smaller contributions to this moment. Therefore, liquid moment coefficient is written as the sum of four terms,

$$
T\,C_{LM} = \tilde{m}_{pl} + \tilde{m}_{pe} + \tilde{m}_{vl} + \tilde{m}_{ve} \,. \tag{28}
$$

The first two terms are the pressure contribution and the remaining two terms are the viscous shear contribution. The fluctuating part of the inviscid $\hat{P}$, which is the primary contributor to the inertial wave motion, is given by

$$
\Delta p = \rho_L\, a^2\, \dot{\phi}^2\, R\left\{ \left[p_I - \frac{rx}{r^2}\hat{K} \right] e^{s\phi - i\theta} \right\} R\left\{ C_p e^{i\phi_p} \hat{K} e^{(s\phi - i\theta)} \right\} . \tag{29}
$$

Calculating the surface integral of this with the appropriate moment arm over the container wall yields the moment contribution due to pressure

$$
\tilde{m}_{pl} + \tilde{m}_{pe} = R\left\{ \begin{array}{l} i\,\frac{1}{2a}\int_{-c}^{c} x\left[C_p e^{i\phi_p} + p_V \right]_{r=a} dx - \\ -i\,\frac{1}{2Ca^2}\int_0^a r^2 C_p e^{i\phi_p}\,\Big|_{x=-c}^{x=c} dr \end{array} \right\} . \tag{30}
$$

The viscous shear moment along the lateral wall is calculated from the boundary layer solutions

$$\tilde{m}_{vl} = \left(2\hat{K}\,Re\right)^{-1} \int_{-C}^{C} \left[ia\frac{\partial w_v}{\partial r} + Cx\frac{\partial u_v}{\partial r} \right]_{r=a} dx\,, \tag{31}$$

while the shear moment due to the end walls is given by

$$\tilde{m}_{ve} = \left(2a\hat{K}\,Re\right)^{-1} \int_{0}^{a} \left[\frac{\partial\left(w_v - i\,v_v\right)}{\partial x} \right]_{x=-C}^{x=C} r\,dr\,. \tag{32}$$

6. Results

The examples given here consider liquid payloads in the M483 Army projectile. The liquid cavity is a cylinder with aspect ratio $C/a = 3$ completely filled with water. This projectile has a gun launch spin rate, $\dot{\phi} = 1500/s$, which is large enough so large Reynolds number boundary layer analysis adequately governs the liquid physics along the entire trajectory. The range of T's for a typical trajectory of the M483 with a frozen (solid) liquid payload is given in figure 3.

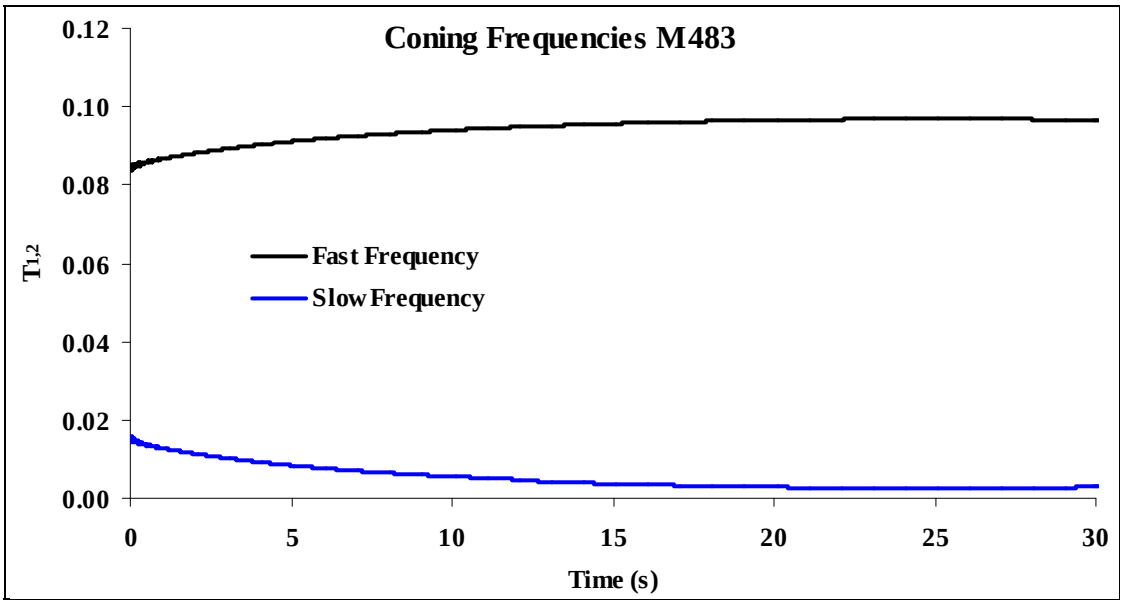

Figure 3. Coning frequency for the M483.

Applying steady-state liquid analysis to this liquid configuration reveals the liquid side moment coefficient C_{LSM} for C/a = 3, for two Reynolds numbers $Re = 5\times10^6, 5\times10^7$ (see figure 4). These results depict typical C_{LSM} behavior where the peaks indicate large overturning liquid moments, possible resonances, generated by this contained liquid as a function of the fast-coning T_1 rate.

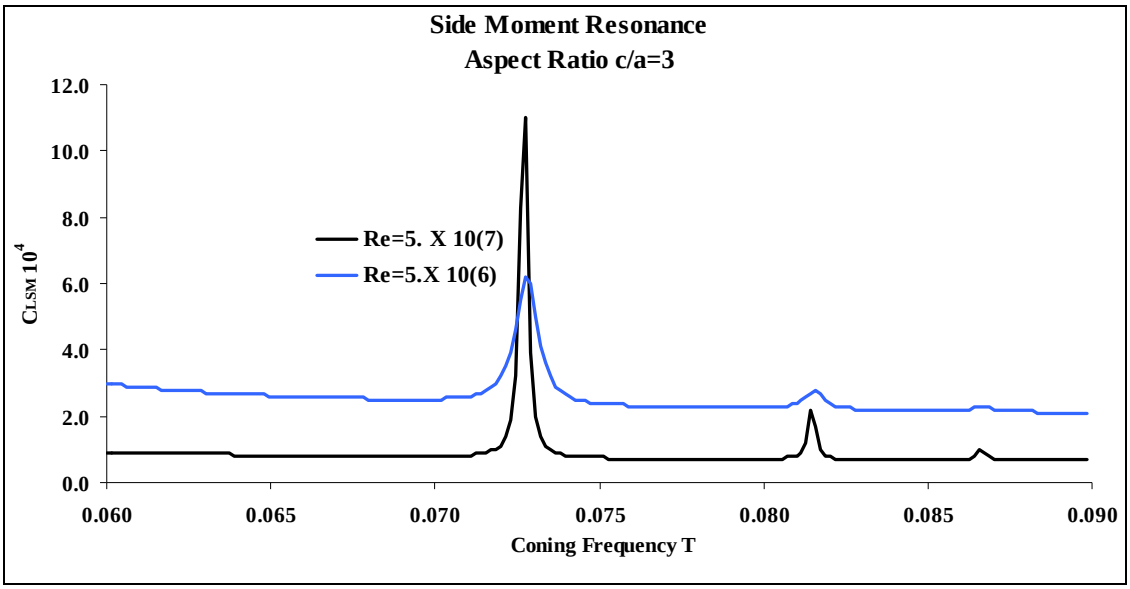

Figure 4. C_{LSM} vs. coning frequency.

This plot suggests that coning frequencies in the neighborhood of T = 0.072 will create significantly larger side moments than those found for frequencies outside this neighborhood. This result is characteristic of the root cause of projectile instabilities due to liquid payloads. The aspect ratio coupled with a large enough Reynolds number will force inertial waves in the coning fluid to generate large overturning liquid moments.[2] Increasing Re causes the liquid side moment to increase rapidly, resulting in a pronounced peak at a resonant frequency.

The range of frequencies given in figure 4 is close to the fast mode T_1 frequencies frozen liquid found in figure 3. This is one indicator that a flowing liquid could cause the fast-coning frequencies to change such that an instability occurs near $T_1 = 0.072$.

Figures 5 and 6 show results of spin rate and roll moment for the M483 comparing a frozen liquid to a flowing liquid payload. The parameters selected for these two plots are chosen because they are strong indicators of flight instability caused by liquid payloads.[2]

This example exhibits no flight instability caused by the liquid moments even with the increased magnitude of Mx. The decreased roll rate and roll moment due to the liquid is a result of the dominance of the fast mode liquid moment for which $C_{LSM} > 0$.

To force flight an instability, take into consideration figure 4 and let the liquid have a decreased viscosity so that the Reynolds numbers all increase during flight. Experience suggests that undamping $\varepsilon_j > 0.6$ means the projectile has encountered flight instability due to liquid moments. An example for the new liquid that generates large overturning moments causing the projectile to go unstable is now discussed. Figure 7 shows the time dependence of the side moment coefficient, $C_{LSM\,1}$, rapidly increasing near $t \approx 11\,s$.

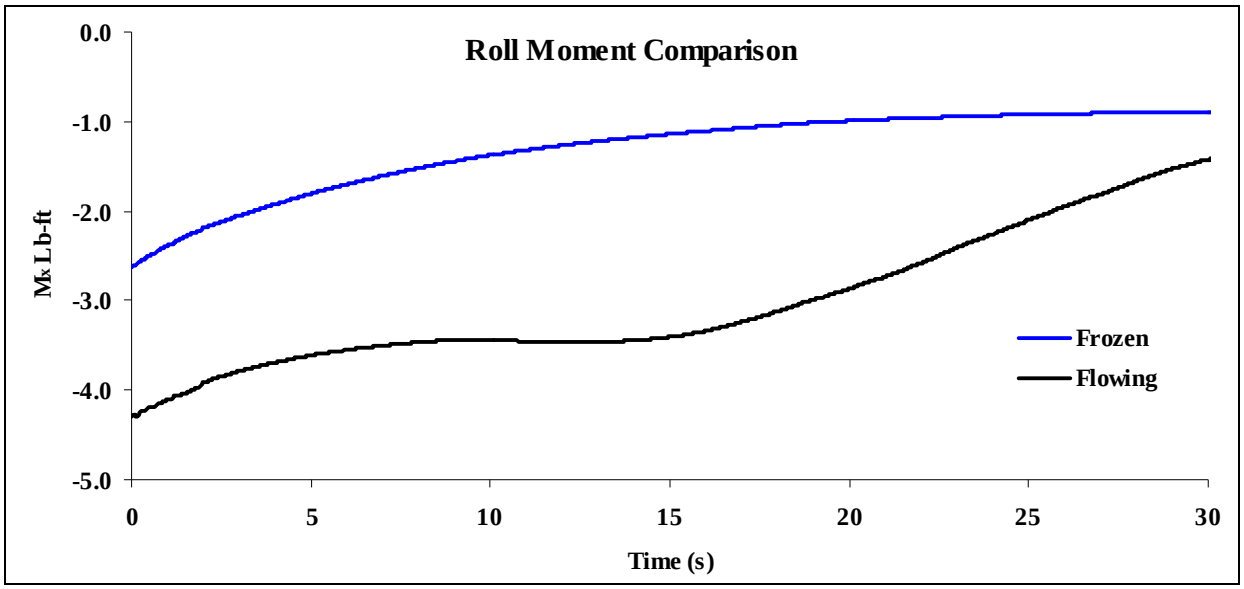

Figure 5. Comparison of projectile roll moment for frozen and flowing liquid.

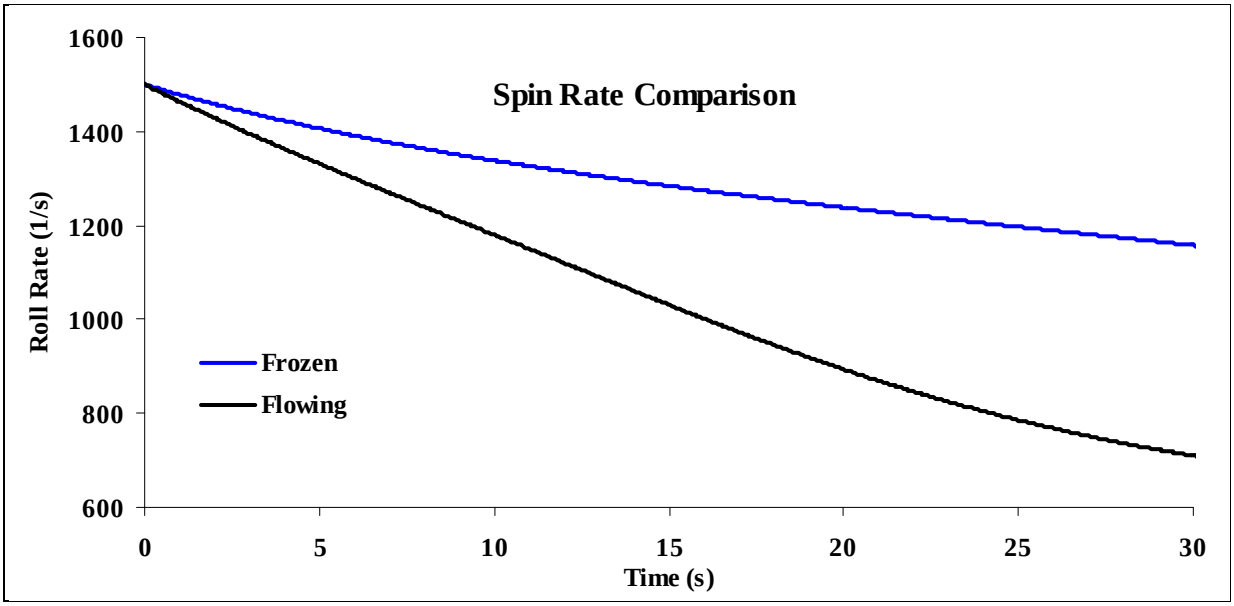

Figure 6. Comparison of projectile spin rate for frozen and flowing liquid.

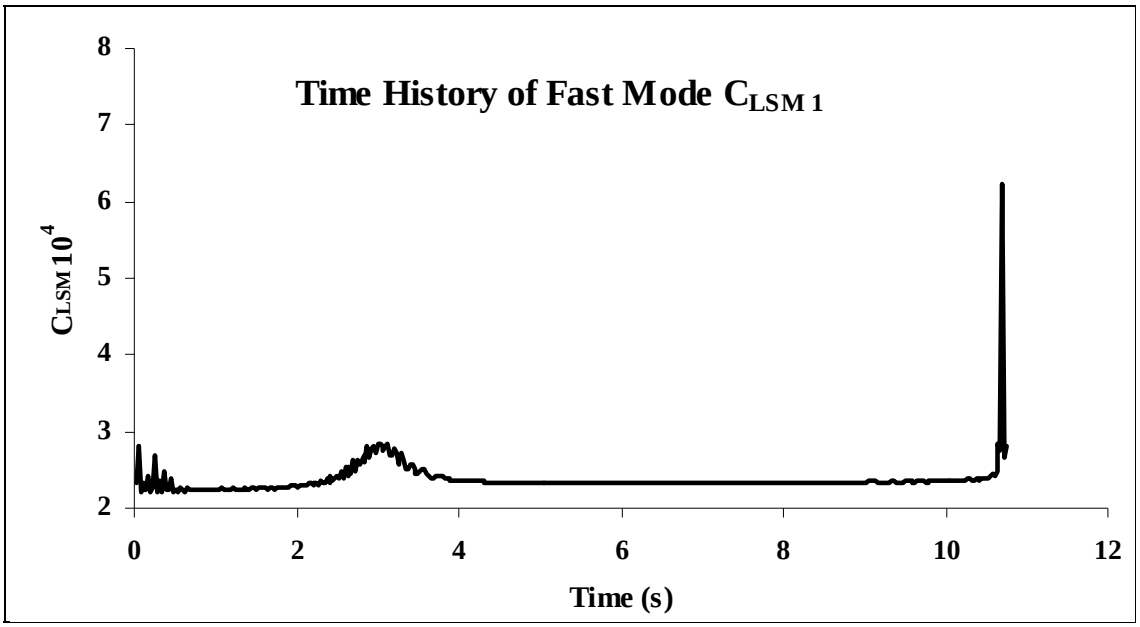

Figure 7. Time history of $C_{LSM\,1}$.

These results again suggest that liquid-induced instability may exist close to t = 11 s, and the cross plot shown in figure 8 reveals a rapid increase in $C_{LSM\,1}$ in the neighborhood of the fast coning rate $T_1 = 0.072$.

Similar results are found for the roll moment coefficient $C_{LRM\,1}$, indicating that the fluid resonance found in figures 7 and 8 is responsible for the large overturning moment, roll moment, and undamping exhibited by the fast frequency coning motion. Figure 9 compares the roll rates of an unstable example, $\varepsilon_1 > 0.6$, which occurs at time $t \approx 11\,s$, and a frozen liquid payload.

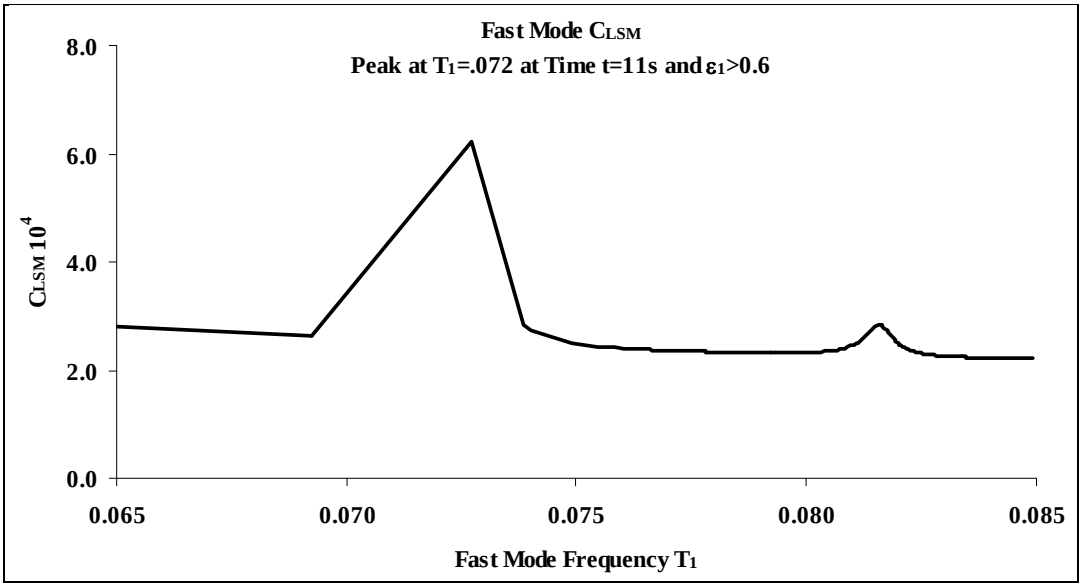

Figure 8. Slow mode C_{LSM} fast coning frequency T_1.

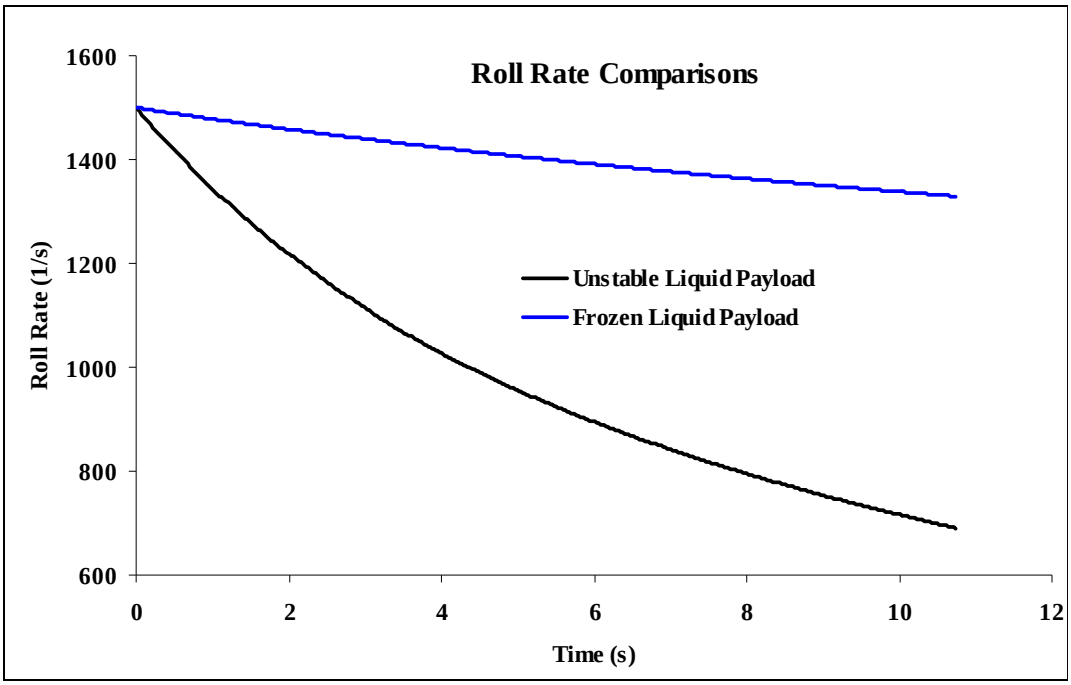

Figure 9. Roll rate vs. time for flowing and frozen liquid payloads.

The rapid decrease in roll rate is caused by the low-viscosity liquid, which is forcing this projectile fast mode coning frequency to approach values close to fast mode resonance near $T_1 \approx 0.072$. Figure 10 presents pitch rates of a projectile with both frozen and flowing low-viscosity liquid payloads. Again, the rapid increase in pitch rate takes place near time $t \approx 11\,s$ in the neighborhood of the fast mode resonant frequency $T_1 = 0.072$. Another indicator of liquid-induced instability is the rapid increase in the angle of attack given in figure 11.

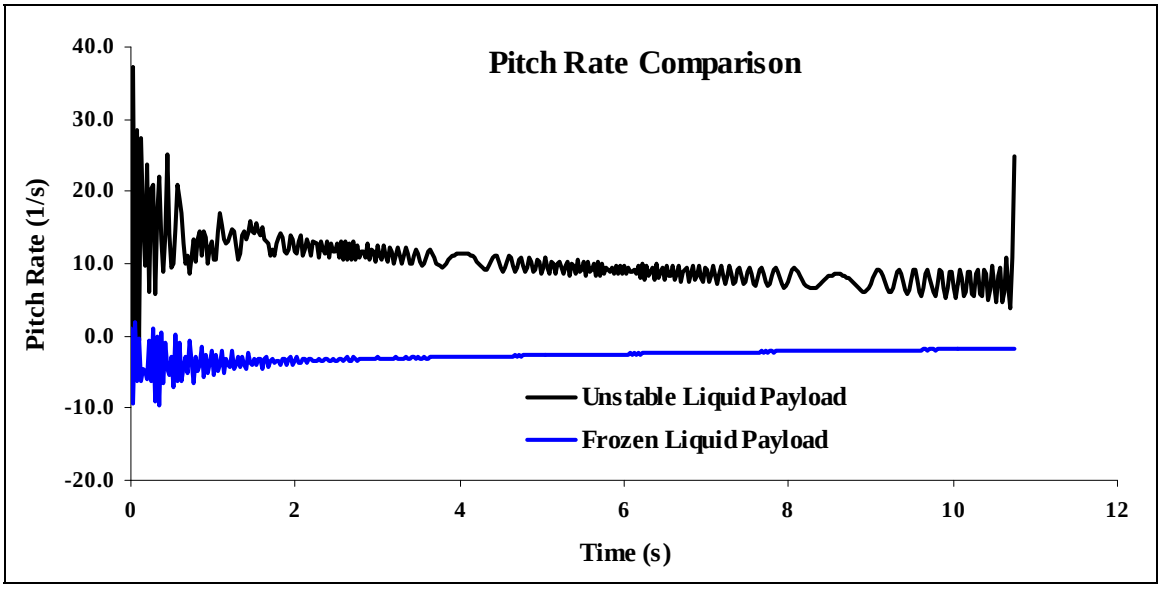

Figure 10. Comparison of pitch rates for flowing and frozen liquid payloads.

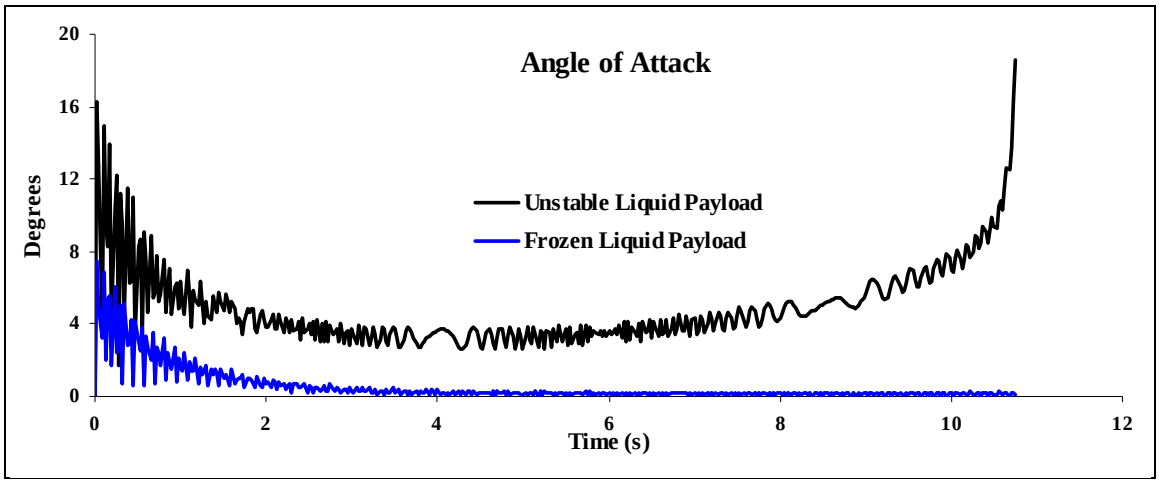

Figure 11. Angle of attack vs. time.

The data displayed in the last five plots provide flight parameters that correspond to flight instability due to the side moment generated by the high Reynolds number liquid payload. In general, these kinds of results occur when the damping rate is $\varepsilon_1 > 0.6$.

7. Conclusion

Liquid moments calculated from linear liquid motion undergoing two-mode steady-state coning motions are used as average moments when applied to a nonlinear 6-DOF time-dependent trajectory model. These quasi-static averages yield approximate predictions describing the motion of projectiles with low-viscosity liquid payloads filling a cylindrical cavity. The magnitudes of the liquid moments are dependent on the two projectile coning frequencies, two projectile coning undamping rates, payload aspect ratio, and the liquid Reynolds number. The nonlinear 6-DOF motion of a projectile is often well approximated as the sum of fast and slow coning motions. Thus, under these conditions the linear liquid analysis can predict when a projectile exhibits flight instability due to a liquid payload by tracking the coning frequencies during the 6-DOF numerical integration process. Even though such predications are based on steady-state theory, they at least serve as an indicator when liquid-induced flight instabilities are likely to exist. This hybrid numerical tool provides reasonable estimates of capturing the physical effects of liquid moments on free-flight projectiles.

List of Symbols, Abbreviations, and Acronyms

a	radius of the cylinder containing fluid
c	half length of the cylinder containing N subcylinders
f_j	$1+2\pi a^4 C\rho/I_x C_{LIM\,j}$
m_L	liquid mass $m_L = 2\pi a^2 C\rho$
$\dot{\phi}$	projectile angular velocity along the projectile axis
$\hat{P}$	liquid pressure perturbation
p	pressure perturbation
s	complex coning frequency $s = (\varepsilon + i)T$
T , T_j	nondimensionalized coning frequency
S_g	gyroscopic stability factor
$\begin{bmatrix} u \\ v \\ w \end{bmatrix}$	liquid perturbation velocity components $\begin{bmatrix} u \\ v \\ w \end{bmatrix} = \begin{bmatrix} \text{axial velocity} \\ \text{radial velocity} \\ \text{azimuthal velocity} \end{bmatrix}$
J **K**	Cartesian unit vectors
$\hat{K}$	coning angle
S_g	gyroscopic stability factor
t	time
δ_a	$=(1+i)\left[2(1+is)\mathrm{Re}\right]^{-1/2}$

δ_c $= -\frac{a/c\,\delta_a}{2\sqrt{1+is}}\left[\frac{1-is}{\sqrt{3+is}} + i\left(\frac{3+is}{\sqrt{1-is}}\right)\right]$

$\varepsilon, \varepsilon_j$ growth rate per cycle

ε_{aj} growth rate per cycle due to aerodynamic moment

μ the dynamic viscosity of liquid

ϕ_j $\phi_{j0} + T_j\dot{\phi}t$

ρ liquid mass density

$\tilde{\vdots}$ variable in nonrolling system

NO. OF
COPIES ORGANIZATION

1 (PDF only) DEFENSE TECHNICAL INFORMATION CTR
DTIC OCA
8725 JOHN J KINGMAN RD
STE 0944
FORT BELVOIR VA 22060-6218

1 DIRECTOR
US ARMY RESEARCH LAB
IMNE ALC HRR
2800 POWDER MILL RD
ADELPHI MD 20783-1197

1 DIRECTOR
US ARMY RESEARCH LAB
RDRL CIM L
2800 POWDER MILL RD
ADELPHI MD 20783-1197

1 DIRECTOR
US ARMY RESEARCH LAB
RDRL CIM P
2800 POWDER MILL RD
ADELPHI MD 20783-1197

ABERDEEN PROVING GROUND

1 DIR USARL
RDRL CIM G (BLDG 4600)

NO. OF
COPIES ORGANIZATION

2 COMMANDER
ARDEC/RDEC
AMSRD AAR AEM C
A READDY
M CORZO
BLDG 94
PICATINNY ARSENAL NJ 07806-5000

1 COMMANDER
ARDEC/RDEC
AMSRD AAR AEM C
K CHUNG
BLDG 407
PICATINNY ARSENAL NJ 07806-5000

5 COMMANDER
ARDEC/RDEC
AMSRD AAR AEM A
B WONG
BLDG 94
PICATINNY ARSENAL NJ 07806-5000

1 COMMANDER
ARDEC/RDEC
AMSRD AAR AEM A
W KOENIG
BLDG 95
PICATINNY ARSENAL NJ 07806-5000

1 M MILLER
504 HAVERHILL RD
JOPPA MD 21085-4319

1 SCHOOL OF AEROSPACE ENGRG
GEORGIA INST OF TECHLGY
M COSTELLO
ATLANTA GA 30332

ABERDEEN PROVING GROUND

1 COMMANDER
US ARMY ECBC
RDRL ECB RT D
WEBER BLDG E3516
D WEBER
APG MD 21010-5424

NO. OF
COPIES ORGANIZATION

8 DIR USARL
RDRL WM
J SMITH
RDRL WML
M ZOLTOSKI
RDRL WML F
D LYON
RDRL WML B
J MORRIS
RDRL WML E
F FRESCONI
G COOPER
B GUIDOS
RDRL WML D
M NUSCA